The Astrophysical Journal Letters, 744:L20 (6pp), 2012 January 10 doi:10.1088/2041-8205/744/2/L20

THE BUTTERFLY EFFECT IN THE EXTREME-MASS RATIO INSPIRAL PROBLEM

Pau Amaro-Seoane[1,2], Patrick Brem[3], Jorge Cuadra[4], and Philip J. Armitage[5]
[1] Max Planck Institut für Gravitationsphysik (Albert-Einstein-Institut), D-14476 Potsdam, Germany; Pau.Amaro-Seoane@aei.mpg.de
[2] Institut de Ciències de l'Espai (CSIC-IEEC), Campus UAB, Torre C-5, parells, 2na planta, ES-08193 Bellaterra, Barcelona, Spain
[3] Astronomisches Rechen-Institut, Mönchhofstraße 12-14, 69120, Zentrum für Astronomie, Universität Heidelberg, Germany; pbrem@ari.uni-heidelberg.de
[4] Departamento de Astronomía y Astrofísica, Pontificia Universidad Católica de Chile, Santiago, Chile; jcuadra@astro.puc.cl
[5] JILA, University of Colorado and NIST at Boulder, 440 UCB, Boulder, CO 80309-0440, USA; pja@jilau1.colorado.edu
Received 2011 August 25; accepted 2011 November 28; published 2011 December 16

ABSTRACT

Measurements of gravitational waves from the inspiral of a stellar-mass compact object into a massive black hole are unique probes to test general relativity (GR) and massive black hole (MBH) properties, as well as the stellar distribution about these holes in galactic nuclei. Current data analysis techniques can provide us with parameter estimation with very narrow errors. However, an extreme-mass ratio inspiral (EMRI) is not a two-body problem, since other stellar bodies orbiting nearby will influence the capture orbit. Any deviation from the isolated inspiral will induce a small, though observable, deviation from the idealized waveform which could be misinterpreted as a failure of GR. Based on conservative analysis of mass segregation in a Milky-Way-like nucleus, we estimate that the possibility that another star has a semimajor axis comparable to that of the EMRI is non-negligible, although probably very small. This star introduces an observable perturbation in the orbit in the case in which we consider only loss of energy via gravitational radiation. When considering the two first-order non-dissipative post-Newtonian contributions (the periapsis shift of the orbit), the evolution of the orbital elements of the EMRI turns out to be chaotic in nature. The implications of this study are twofold. From the one side, the application to testing GR and measuring MBH parameters with the detection of EMRIs in galactic nuclei with a millihertz mission will be even more challenging than believed. From the other side, this behavior could in principle be used as a signature of mass segregation in galactic nuclei.

Key words: galaxies: nuclei – gravitational waves – stars: kinematics and dynamics

Online-only material: color figure

1. MOTIVATION

A stellar mass black hole or neutron star executes $\sim 10^5$–10^6 orbits during the final year of inspiral toward a $\sim 10^6\,M_\odot$ supermassive black hole (MBH). The large number of cycles implies that a phase-coherent measurement of the inspiral, achievable through detection of low frequency gravitational waves, would be a tremendously powerful probe of the space-time near a black hole (Amaro-Seoane et al. 2007; Hughes 2009). Among other things, it would enable a precise determination of the spin of the supermassive black hole and a test of general relativity (GR) that is independent of current constraints derived from pulsar timing data.

There is no foreseeable instrument sensitive enough to detect gravitational waves from extreme-mass ratio inspirals (EMRIs) over timescales comparable to the orbital period. As a consequence, realizing the astrophysical and gravitational physics promise of EMRIs requires an assurance that the inspiral can be accurately modeled over many orbits using templates calculated by solving the two-body problem in GR (for a review, see, e.g., Barack 2009). It is therefore necessary to assess whether gas, stars, or other compact objects in the vicinity could significantly perturb EMRI trajectories. In the case of gas, perturbations to stellar mass black holes or neutron stars[6] are securely negligible provided that accretion onto the black hole occurs in a low density, radiatively inefficient flow (Narayan 2000). Such flows are much more common than dense accretion disks, which *would* yield observable phase shifts during inspiral (Kocsis et al. 2011), at least at the relatively low redshifts where EMRIs may be observed.

In this Letter, we quantify the nature and strength of possible perturbations from point mass perturbers: low-mass stars or compact objects in tight orbits around the supermassive black hole. Any perturbers are unlikely to orbit close enough to the EMRI to undergo strong interactions, so the regime of interest is one where the third body is relatively distant and the interaction is weak. The Newtonian analog of this problem has been studied extensively in the context of both solar system satellite evolution and for transit timing variations of extrasolar planets (Dermott et al. 1988; Agol et al. 2005; Holman & Murray 2005; Veras et al. 2011). In Newtonian gravity, perturbations are strong only at the location of mean motion resonances, and these have the effect of inducing small jumps in eccentricity upon divergent resonance crossing. This would already be interesting for the EMRI problem, since the jumps in eccentricity would result in a perturbation to the gravitational wave decay rate and an eventual dephasing of the waveform. However, as we will see, the inclusion of post-Newtonian corrections changes the evolution qualitatively. Computing trajectories that include the two first-order non-dissipative post-Newtonian corrections, we find evidence of dependence on initial conditions in the evolution of the perturbed inner binary, such that arbitrarily small variations in the initial orbit lead to significantly different future behavior.

2. ASTROPHYSICAL LIMITS ON PERTURBERS

Is it likely that a star or compact object will be present close enough to perturb the orbit of an EMRI? Excluding low-mass MBHs ($M_\bullet < 10^6\,M_\odot$), where the stellar tidal disruption limit

[6] White dwarf EMRIs are excluded here because mass loss from the compact object itself could form a dynamically significant disk even if the background accretion flow is of low density (Zalamea et al. 2010).

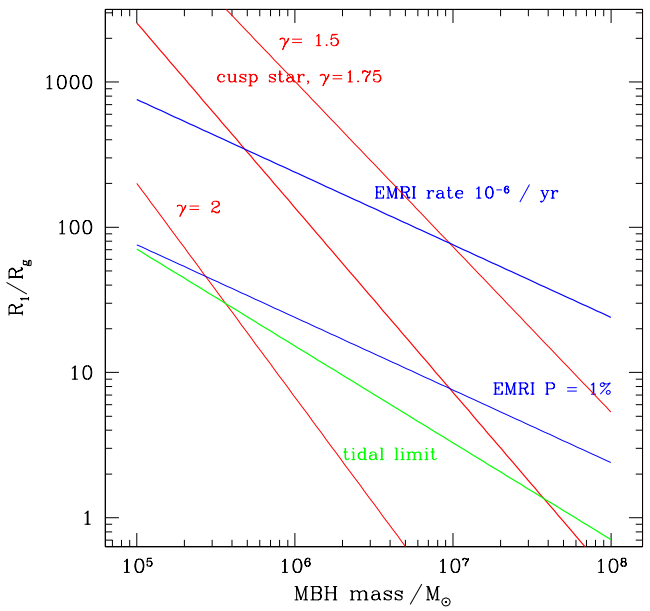

Figure 1. Estimates for the semimajor axis of the innermost perturbing body around a massive black hole, scaled to the hole's gravitational radius $R_g = GM_\bullet/c^2$. The red lines show the location of the innermost star, estimated assuming that stars of mass 0.3 $M_\odot$ follow a single power-law cusp of index γ in a galaxy on the $M_\bullet$–σ relation. The green line shows the tidal disruption limit for such stars. The blue lines show the average (upper) and 1% probability (lower) location of the next nearest EMRI, assuming uncorrelated inspirals at a rate of 10^{-6} yr^{-1}.

comes into play, the existence of perturbers is not excluded by elementary arguments. Neither, however, is it easy to calculate the probability distribution of perturbers, whose proximity will depend upon the details of discreteness and relativistic effects very close to the MBH and mass segregation and EMRI injection mechanisms in galactic nuclei (Preto et al. 2004; Freitag et al. 2006; Amaro-Seoane et al. 2004; Alexander & Hopman 2009; Preto & Amaro-Seoane 2010; Amaro-Seoane & Preto 2011).

Rather than facing these difficulties, we limit ourselves here to order of magnitude estimates for the likely location of the nearest star and compact object. For stars, assumed to be of a single mass M_*, we assume a cusp-like distribution with a density profile $\rho \propto R^{-\gamma}$, extending from the MBH to its radius of influence $R_{\rm BH} = GM_\bullet/\sigma^2$. Here σ is the velocity dispersion of the galaxy. Using the fact that the enclosed mass, $M(R) \simeq M_\bullet$ at $R = R_{\rm BH}$, we find that the expected radius of the innermost star, R_1, is

$$\frac{R_1}{R_g} = \left(\frac{M_*}{M_\bullet}\right)^{1/(3-\gamma)} \left(\frac{c}{\sigma}\right)^2, \qquad (1)$$

where $R_g = GM_\bullet/c^2$. This formula yields an explicit estimate for R_1 once we adopt a relation between $M_\bullet$ and σ (Gültekin et al. 2009). For the location of the next nearest compact object (or EMRI), we use an even simpler approach. We calculate the expected semimajor axis for uncorrelated inspirals due to gravitational radiation (Peters 1964), assuming near-circular orbits and rate $\dot{N}_{\rm EMRI}$. Finally, we plot the tidal limit (e.g., Rees 1988) for 0.3 $M_\odot$ main-sequence stars.

Figure 1 shows these estimates as a function of $M_\bullet$. For a standard cusp slope $\gamma = 1.75$, there is likely to be a low-mass stellar perturber within a few hundred R_g for $M_\bullet > 10^6\,M_\odot$. Similarly, if the EMRI rate is as high as 10^{-6} yr^{-1}, there

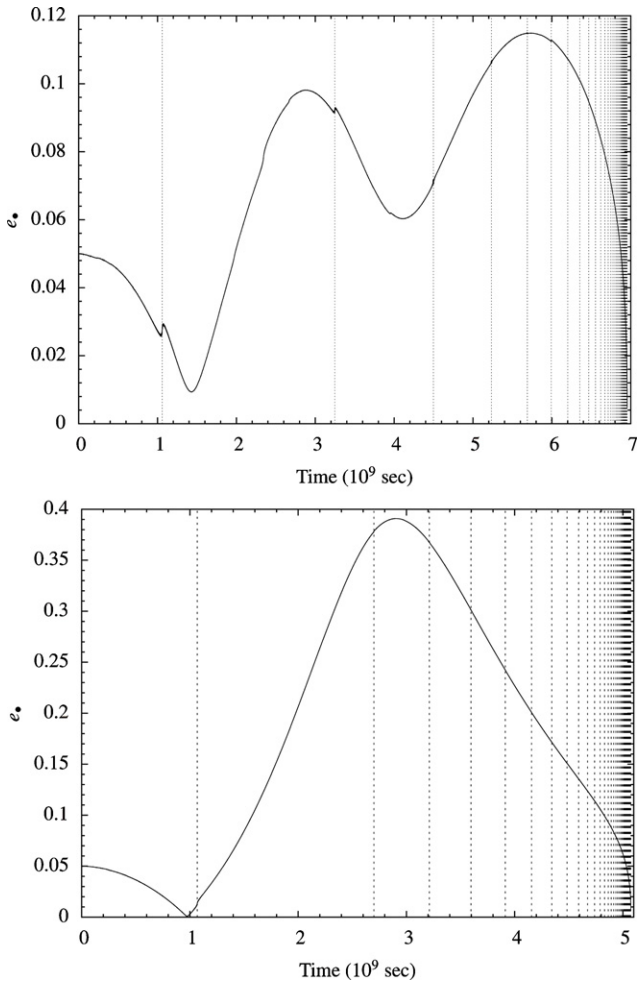

Figure 2. Upper panel: results for the fiducial case using the direct-summation N-body integrator. The mass of the MBH is $\mathcal{M}_\bullet = 10^6\,M_\odot$, the mass of the stellar black hole is $m_\bullet = 10\,M_\odot$. See the text for more details. Lower panel: same configuration but with an initial inclination of the star of $i_\star = 45^\circ$ instead of 30°, i.e., the inclination triggers the Kozai mechanism, since $i_\star > 39.^\circ 2$ *and* the orbit is prograde. As mentioned in the previous case, even if the changes in eccentricity cannot be directly seen in the curve, they are of the order $\Delta e_\bullet \sim 10^{-3}$.

is a significant chance (at least a few percent) that a second compact object will be present between 10 and 10^2 R_g for $10^6\,M_\odot < M_\bullet < 10^7\,M_\odot$. Clearly, these crude estimates do not demonstrate that *most* EMRIs will be perturbed by third bodies, but they do suggest that perturbers may be close enough in some galaxies to motivate detailed consideration of their dynamical effects.

3. METHODS

We are interested in the secular effect of a star acting on an EMRI which will describe thousands of orbits in the detector bandwidth and slowly decay. The kind of effects on the wave that we are looking at are tiny, though detectable, and the mass difference between the two binaries (the MBH–EMRI and the MBH–star systems) is huge. We therefore need a numerical tool capable of integrating the plunging orbit of the EMRI while inducing a minimal error in the integration, since data analysis techniques can detect, e.g., eccentricity differences of the order $\Delta e \sim 10^{-3}$ (Amaro-Seoane et al. 2010; Porter & Sesana 2010; Key & Cornish 2011). Hence, we have chosen to use a direct

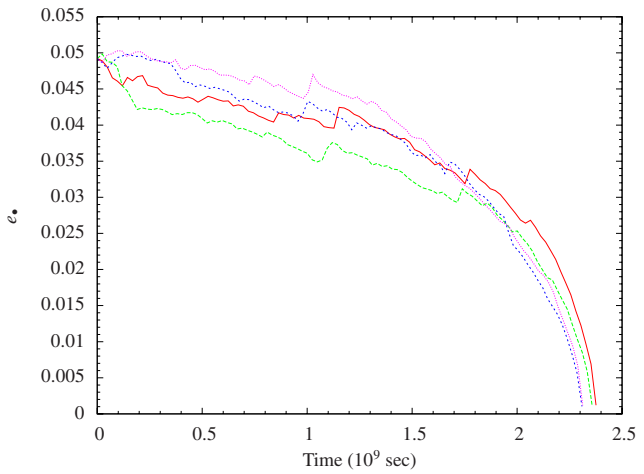

Figure 3. Fiducial case with energy dissipation and periapsis shift correcting terms for different initial inclinations of the perturber. The solid (red) curve corresponds to $i_\star = 30^\circ$, the long-dashed curve (green) to $i_\star = 30.^\circ001$, the short-dashed curve (blue) corresponds to the fiducial case plus a *billionth* of a degree, $i_\star = 30.^\circ0000000001$, and the dotted curve (magenta) to the reference plus a 10^{-13} of a degree, $i_\star = 30.^\circ0000000000001$.

(A color version of this figure is available in the online journal.)

N-body approach (Aarseth 1999, 2003), the `planet` code, written by Aarseth.[7] This is the most expensive method because it involves integrating all gravitational forces for all three bodies at every time step, without making any a priori assumptions about the system. Our approach employs the improved Hermite integration scheme, which requires computation of not only the accelerations but also their time derivatives. Since we are simply integrating Newton's equations directly, all gravitational effects are included. For the purpose of our study, nonetheless, we have included relativistic corrections to the Newtonian forces (the forces can be found in the same page in the `toy` code[8]). This was first implemented in a direct-summation N-body code by Kupi et al. (2006). For this, one has to add perturbations in the integration, so that the forces are modified by

$$F = \overbrace{F_0}^{\text{Newt.}} + \overbrace{\underbrace{c^{-2}F_2}_{\text{1PN}} + \underbrace{c^{-4}F_4}_{\text{2PN}}}^{\text{periapsis shift}} + \overbrace{\underbrace{c^{-5}F_5}_{\text{2.5PN}}}^{\text{energy loss}} + \overbrace{\mathcal{O}(c^{-6})}^{\text{neglected}}. \quad (2)$$

In the last equation "PN" stands for post-Newtonian. We note that the perturbations do not need to be small compared to

[7] Who, as is his admirable custom, has made the code publicly available http://www.ast.cam.ac.uk/~sverre/web/pages/nbody.htm.

[8] ftp://ftp.ast.cam.ac.uk/pub/sverre/toy/README

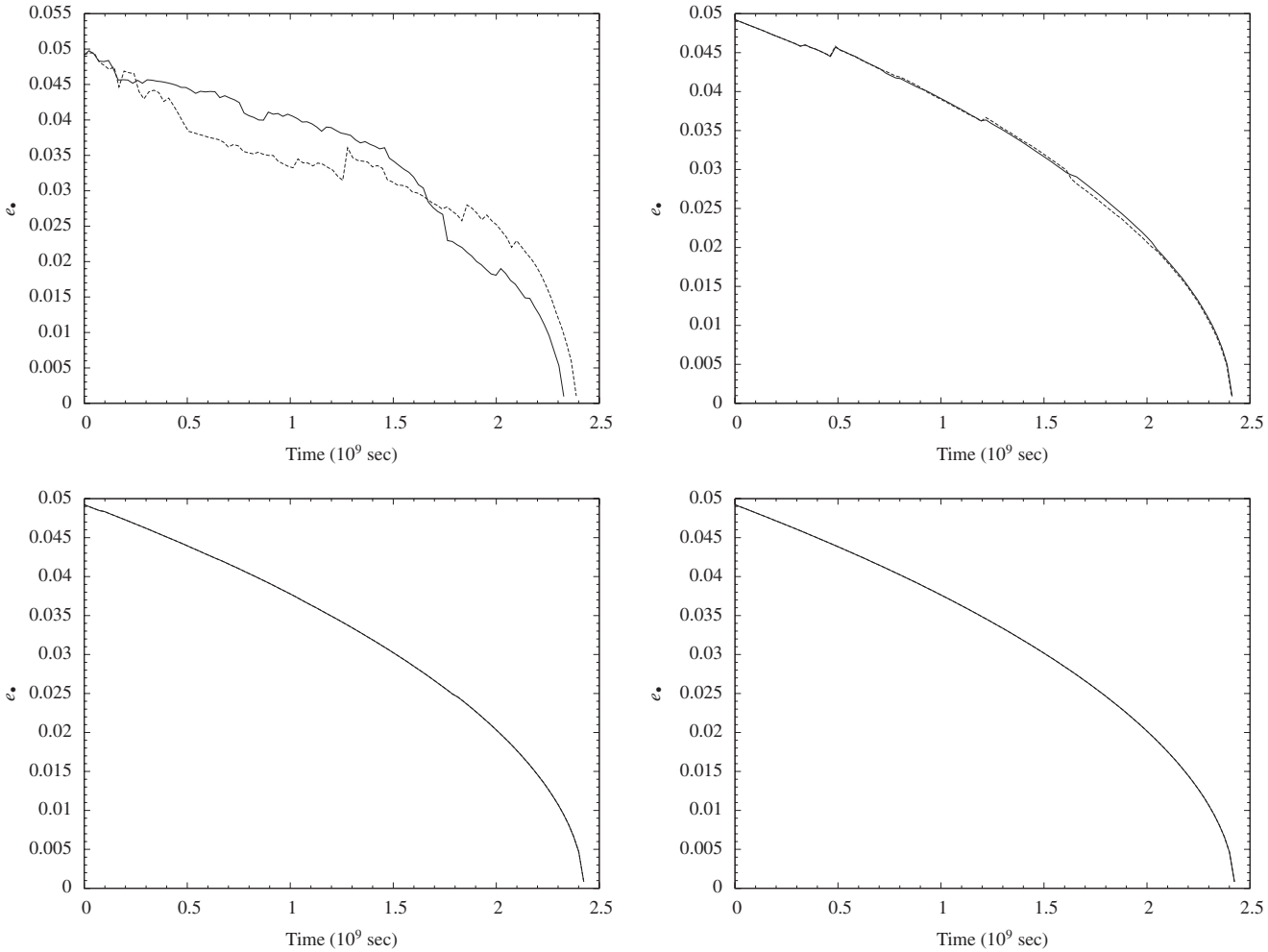

Figure 4. Same as in Figure 3 but we set initially the perturber at a larger and larger initial semimajor axis. From the top to bottom and from the left to the right, the semimajor axis of the perturber is $a_\star = 4 \times 10^{-6}$ pc, 6×10^{-6} pc, 9×10^{-6} pc, and 4.07243×10^{-5} pc. Solid lines correspond to $i_\star = 30^\circ$ and dashed lines to $i_\star = 30.^\circ0000000001$.

the two-body force (Mikkola 1997). The expressions for F_2, F_4, and F_5 can be found in Blanchet & Faye (2001), their Equation (7.16).

4. DISSIPATION OF ENERGY AND RESONANCES

We first analyze the system by contemplating only the relativistic effect of dissipation of energy, i.e., our simulations only incorporate the 2.5PN correction term. We stop the integration when the separation between the stellar BH and the MBH is $a_\bullet = 5\,R_{\rm Schw}$, which approximately corresponds to the limit where the PN approximation is not valid anymore. The inspiral down to this distance typically takes some 440,000 orbits in our simulations.

In Figure 2 the test stellar black hole of mass $m_\bullet = 10\,M_\odot$ has been initially set in such an orbit that it is totally embedded in a LISA-like detector band (i.e., with an orbital period $<10^5$ s, namely, $P_\bullet = 6 \times 10^3$ s) and is hence an EMRI; its initial semimajor axis is $a_{\bullet,\,\rm i} \simeq 1.45 \times 10^{-6}$ pc and its eccentricity is $e_{\bullet,\,\rm i} = 0.05$. The perturber, a star of mass $m_\star = 10\,M_\odot$, is initially on an orbit in which the semimajor axis has the value $a_{\star,\,\rm i} \simeq 4.1 \times 10^{-6}$ pc and the eccentricity at $T = 0$ is $e_{\star,\,\rm i} = 0.5$. The inclination of the system EMRI–star was set to 30° initially in the upper panel. This constitutes our reference system.

In the figure, the straight lines mark the condition $P_\star/P_\bullet = A$, with A an integer, $P_\star$ the period of the star around the MBH, and $P_\bullet$ the period of the EMRI around the MBH, i.e., where the resonances occur. The first three resonances have an impact on $e_\bullet$ which can be seen on the plot; later resonances also affect $e_\bullet$, with $\Delta e_\bullet \sim 10^{-3}$. We also note that in the upper panel one can see in between smaller jumps; they correspond to higher-order resonances, $P_\star/P_\bullet = 5.5$, 6.5, and 7.5.

We made the choice for an initial inclination of 30° to avoid another effect that introduces a change in the eccentricity. In the lower panel we have *exactly* the same system but for $i_\star = 45^\circ$. With this value, and the fact that the orbit is prograde, the Kozai oscillation of eccentricity is present (Kozai 1962). Even if the eccentricity of the EMRI $e_\bullet$ suffers the characteristic Kozai oscillations, the loci for the resonances still fulfill the condition $P_\star/P_\bullet =$ integer.

5. DOES THE FLAP OF THE STAR AT APOAPSIS SET OFF A TORNADO AT PERIAPSIS?

In this subsection we address numerically the effect of including the relativistic periapsis shift along with the dissipation of energy, i.e., the set of corrections as specified in Equation (2). As we show below, the effect of the periapsis shift completely changes the evolution of the system. In Figure 3, we show four cases. One corresponds to the reference system but taking into account the periapsis shift. We only display these examples but note that the behavior is also chaotic[9] for other nearby choices of $i_\star$. When using an initial inclination of $i_\star = 45^\circ$, which corresponds to the same situation as in the lower panel of Figure 2 but taking into account the periapsis shift, along with another case which is identical except that $i_\star = 45.^\circ0000000001$, we also find a chaotic result which moreover eliminates the secular Kozai oscillation of e.

We have systematically studied this chaotic behavior by running hundreds of simulations in which we methodically increase in minimal differences an initial dynamical orbital parameter such as the inclination, semimajor axis, or eccentricity. In all cases and parameters the evolution corroborates the chaotic behavior of the system. We have also tested a mass for the perturbing star of 5 and $1.44\,M_\odot$, as well as different values of $e_\star$ (0.1, 0.3, 0.7, and 0.9), with similar results.

In order to fence in the region within which the system is chaotic, we systematically increase the semimajor axis of the star and run the same experiment. We start with the same difference in inclination at a slightly larger semimajor axis, and then regularly increase it until we reach one order of magnitude over the fiducial case, as we depict in Figure 4. The chaotic behavior ceases at about one order of magnitude of the initial value of $a_\star$ in the reference case.

6. QUANTIFYING THE DEPENDENCE ON INITIAL CONDITIONS OF THE SYSTEM

In this section, we present a way of systematically characterizing the rate of separation of infinitesimally close trajectories. To achieve this we compare our fiducial model with another case in which we set up the EMRI in an (almost) imperceptibly different initial orbit (the initial difference is 2×10^{-10} pc, while the objects are moving on the same ellipse) and keep the same initial conditions of the MBH and the perturber. Hence, the EMRI in the second case differs only from the reference case slightly and has an initial distance separation of r_0. We say that the two models are in phase provided that

$$r \approx r_0. \tag{3}$$

If the two different realizations reach a separation

$$r \approx 2\,a_\bullet, \tag{4}$$

the EMRI bodies are moving out of phase on entirely unrelated orbits. We thence are able to estimate a characteristic timescale $\tau_{\rm deph}$ for the system to become out of phase. In Figure 5 we display the separation of the two systems for different distances to the perturber. From these figures we can measure the value of a characteristic timescale $\tau_{\rm deph}$ for a given $a_\star$.

From the data points obtained in the upper panels of Figure 5 we can then derive the relation displayed in the lower panel. For large enough distances, of the order of $\sim 10^{-5}$ pc, the two timescales converge and the system becomes deterministic.

7. CONCLUSIONS

In this paper, we have addressed the role of a perturbation on an EMRI by a nearby star. The system depends extremely on *minimal* changes in the initial conditions (as small as a 10^{-9} part in the inclination) leading to a very different dynamical evolution. In all cases, however, the Kozai mechanism is washed out by the periapsis shift, as one can expect (see, e.g., Holman et al. 1997; Blaes et al. 2002). For distances of the order of $a_\star \sim 10^{-5}$ pc the system enters the chaotic regime, for perturbing masses as small as $1.44\,M_\odot$. While we cannot state clearly whether this will be a common feature for EMRIs, since the different dynamical and relativistic phenomena involved in the problem are many and not straightforward (for a review, see Amaro-Seoane et al. 2007 and P. Amaro-Seoane 2012, in preparation for a dedicated review of the dynamics), it seems plausible that for a Milky-Way-like galaxy a star can be at such

[9] When we use the word, we do not follow the rigorous mathematical definition of chaos. We mean a strong dependence on the initial conditions.

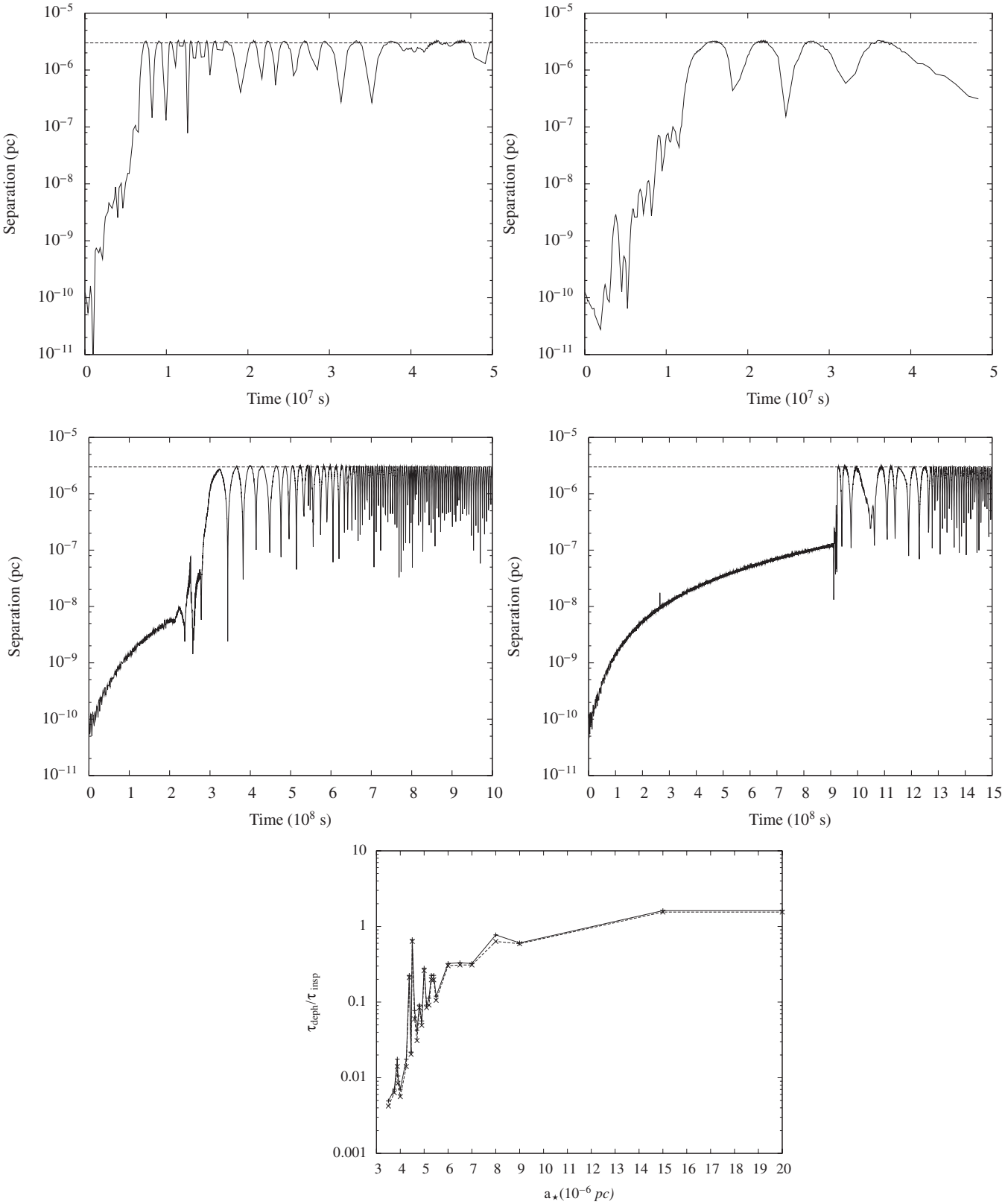

Figure 5. Upper panels: from the left to the right and from the top to the bottom we show the separation r for an increasing separation of the perturbing star of 3.5×10^{-6}, 3.9×10^{-6}, 4.375×10^{-6}, and 4.5×10^{-6} pc. The dashed line shows the critical distance $2\,a_\bullet$. Note the different timescales in the lower panels. Lower panel: $\tau_{\rm deph}$ against distance to the perturber normalized to the gravitational radiation timescale of the isolated system $\tau_{\rm insp}$; i.e., the merger timescale without the perturber acting onto the binary MBH-EMRI.

a radius from the EMRI system that it will significantly perturb it. From the standpoint of detection and data analysis, this is yet another complication of the problem and could even lead to the misinterpretation that nature's GR is not what we believe it to be. On the other hand, from the point of view of stellar dynamics, the detection of one of these systems would shed light on our current understanding of galactic dynamics in general and mass segregation in particular.

We thank Marc Freitag and Rainer Schödel for comments on the manuscript. P.J.A. acknowledges support from the NSF (AST-0807471), from NASA's Origins of Solar Systems program (NNX09AB90G), and from NASA's Astrophysics Theory program (NNX11AE12G). P.A.S. and J.C. were supported in part by the National Science Foundation under Grant No. 1066293 and thank the hospitality of the Aspen Center for Physics. J.C. acknowledges support from FONDAP (15010003), FONDECYT (11100240), Basal (PFB0609), and VRI-PUC (Inicio 16/2010), and the hospitality of JILA, AEI, and MPE. P.B. and P.A.S. acknowledge financial support for research visits in China by The Silk Road Project (2009S1-5) of Chinese Academy of Sciences, National Astronomical Observatories of China and P.B. also acknowledges the University of Heidelberg for travel costs through the excellence initiative ZUK 49/1, TP 14.8 International Research. It is a pleasure for P.A.S. to thank Sabine Pendl for her extraordinary support at the Rote Insel during the preparation of this work and also for her interest in nonlinear dynamics and complex systems, which motivated very interesting discussions.

REFERENCES

Aarseth, S. J. 1999, PASP, 111, 1333
Aarseth, S. J. 2003, Gravitational N-Body Simulations (Cambridge: Cambridge Univ. Press)
Agol, E., Steffen, J., Sari, R., & Clarkson, W. 2005, MNRAS, 359, 567
Alexander, T., & Hopman, C. 2009, ApJ, 697, 1861
Amaro-Seoane, P., Eichhorn, C., Porter, E. K., & Spurzem, R. 2010, MNRAS, 401, 2268
Amaro-Seoane, P., Freitag, M., & Spurzem, R. 2004, MNRAS, 352, 655
Amaro-Seoane, P., Gair, J. R., Freitag, M., et al. 2007, Class. Quantum Grav., 24, R113
Amaro-Seoane, P., & Preto, M. 2011, Class. Quantum Grav., 28, 094017
Barack, L. 2009, Class. Quantum Grav., 26, 213001
Blaes, O., Lee, M. H., & Socrates, A. 2002, ApJ, 578, 775
Blanchet, L., & Faye, G. 2001, Phys. Rev. D, 63, 062005
Dermott, S. F., Malhotra, R., & Murray, C. D. 1988, Icarus, 76, 295
Freitag, M., Amaro-Seoane, P., & Kalogera, V. 2006, ApJ, 649, 91
Gültekin, K., Richstone, D. O., Gebhardt, K., et al. 2009, ApJ, 698, 198
Holman, M. J., & Murray, N. W. 2005, Science, 307, 1288
Holman, M., Touma, J., & Tremaine, S. 1997, Nature, 386, 254
Hughes, S. A. 2009, ARA&A, 47, 107
Key, J. S., & Cornish, N. J. 2011, Phys. Rev. D, 83, 083001
Kocsis, B., Yunes, N., & Loeb, A. 2011, Phys. Rev. D, 84, 024032
Kozai, Y. 1962, AJ, 67, 591
Kupi, G., Amaro-Seoane, P., & Spurzem, R. 2006, MNRAS, 371, L45
Mikkola, S. 1997, Celest. Mech. Dyn. Astron., 68, 87
Narayan, R. 2000, ApJ, 536, 663
Peters, P. C. 1964, Phys. Rev., 136, 1224
Porter, E. K., & Sesana, A. 2010, Phys. Rev. D., submitted (arXiv:1005.5296)
Preto, M., & Amaro-Seoane, P. 2010, ApJ, 708, L42
Preto, M., Merritt, D., & Spurzem, R. 2004, ApJ, 613, L109
Rees, M. J. 1988, Nature, 333, 523
Veras, D., Ford, E. B., & Payne, M. J. 2011, MNRAS, 727, 74
Zalamea, I., Menou, K., & Beloborodov, A. M. 2010, MNRAS, 409, L25